

Bonding and pressure-tunable interfacial thermal conductance

Meng Shen,¹ William J. Evans,² David Cahill,³ and Pawel Koblinski^{1,*}

¹*Department of Materials Science and Engineering, MRC246, Rensselaer Polytechnic Institute, Troy, New York 12180*

²*Rensselaer Nanotechnology Center, Rensselaer Polytechnic Institute, Troy, New York 12180*

³*Frederick-Seitz Materials Research Laboratory, University of Illinois, Urbana, Illinois 61801, USA and
Department of Materials Science and Engineering, University of Illinois, Urbana, Illinois 61801, USA*

(Received 29 May 2011; published 8 November 2011)

Stiffness of interfacial bonding between two materials plays a major role in controlling the thermal conductance of the interface. We use nonequilibrium molecular dynamics simulations to study interfacial thermal conductance at an epitaxial interface between two fcc crystals with interatomic interactions described by Lennard Jones (LJ) potentials. The interface stiffness was varied by two different methods: (i) application of pressure and (ii) direct change of the interfacial bonding strength by varying the depth of potential well parameter of the LJ potential. Our results show that when the interfacial bonding strength is low, interfacial stiffness increases linearly with pressure due to the anharmonicity of atomic interactions. Consequently, the interfacial conductance increases, first proportionally to interfacial stiffness, and then it saturates at a high value. Quantitatively similar behavior is observed when the stiffness of the interfacial bonding is increased by directly varying the depth of the potential well parameter of the LJ potential. By contrast, when the interfacial bonding strength is high, thermal conductance is almost pressure independent and in fact slightly decreases with increasing pressure. This decrease can be explained by the change of overlap between the vibrational density of states (DOS) in the two crystalline materials.

DOI: [10.1103/PhysRevB.84.195432](https://doi.org/10.1103/PhysRevB.84.195432)

PACS number(s): 68.35.Ja

I. INTRODUCTION

Resistance to heat flow posed by the presence of interfaces is important in nanostructured materials characterized by high density of interfaces. In fact interfaces can limit thermal conductivity of nanostructured materials. For example, because of weak thermal coupling between nanotubes (CNT) and a polymer matrix, CNT-polymer composites are characterized by relatively small increases in thermal performance due to introduction of highly conductive fibers, as compared with their pure polymer counterparts.¹ The thermal resistance of interfaces can be affected by the mechanical properties of the materials on each side of the interface,² the atomic-level details of the interfacial structure,³ and the stiffness of interfacial bonds.⁴

The role of interfaces on thermal transport can be quantified by the interfacial thermal resistance R , or its inverse, the interfacial thermal conductance σ . This quantity is defined via

$$J_Q = \sigma \Delta T, \quad (1)$$

where ΔT is a discontinuous temperature drop at the interface, and J_Q is the heat flux across the interface.² The importance of the interfacial resistance can be most easily gauged via the concept of the Kapitza length (l_K), i.e., the equivalent thickness of a bulk material forming the interface that has the same overall thermal resistance as the interface. For carbon nanotubes surrounded by surfactants and dispersed in water, G_K , measured by transient laser-heating methods, as well as modeled via molecular dynamics (MD) simulations, can be as low as 10–20 MW/m² K corresponding to $l_K = 30$ –60 nm.⁵ In this context it is imperative to design approaches to decrease interfacial thermal resistance.

The acoustic mismatch model (AMM) and diffusive mismatch model (DMM) have traditionally provided a basis for understanding the interfacial thermal resistance. These

models provide prescriptions for calculating the transmission coefficient of a phonon with which the interfacial conductance can be evaluated via^{2,6}

$$\sigma(T) = \frac{1}{2} \int_0^\infty D(\omega) \hbar \omega \frac{\partial n(\omega, T)}{\partial T} \langle v_z(\omega) \rangle \langle t(\omega) \rangle d\omega, \quad (2)$$

where $\sigma(T)$ is thermal conductance, $D(\omega)$ is the frequency-dependent vibrational phonon density of states (DOS) per unit volume, $n(\omega, T)$ is the Bose-Einstein occupation number, $\langle v_z(\omega) \rangle$ is the average value of phonon-group velocity at frequency ω in the cross-plane direction, and $\langle t(\omega) \rangle$ is the transmission coefficient of phonons.⁶ While both AMM and DMM provide values for transmission coefficients, neither of the models explicitly accounts for the effect of the stiffness of interfacial bonding on the interfacial heat transfer.

The importance of the stiffness of the interfacial bonding on the transmission coefficients can be easily demonstrated by a theoretical treatment of a simple model of an infinite one-dimensional chain of masses connected by springs.^{6,7} In this simple model half of the chain is composed of masses m_1 connected by springs with stiffness k_{11} , and the other half is composed of masses m_2 connected by springs with stiffness k_{22} . The stiffness of the “interfacial” spring is k_{12} . Using the Caroli formula,⁷ the transmission coefficient can be calculated as⁴

$$\alpha(\omega) = 4k_{12}^2 k_{11} k_{22} \sin(q) \sin(q') / |d|^2, \quad (3)$$

where $t(\omega)$, as before, is the transmission coefficient at frequency ω ; k_{ij} is the generalized spring constant between an atom of type i and an atom of type j ; q and q' are the wave numbers on each side of the interface; and d is a function of spring constants, frequency, and the wave number given by⁴

$$d = [\omega^2 - k_{12} + k_{11}(e^{iq} - 1)][\omega^2 - k_{12} + k_{22}(e^{iq'} - 1)]. \quad (4)$$

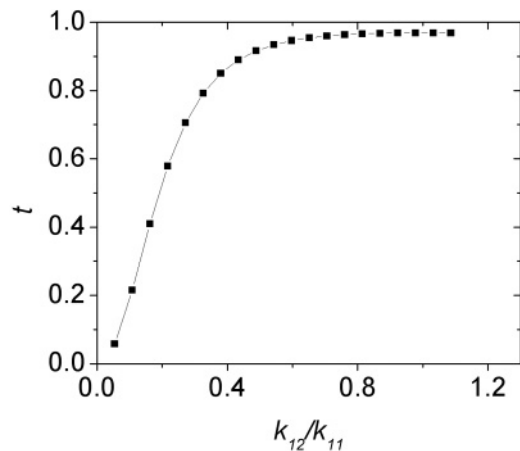


FIG. 1. Energy transmission coefficient as a function of normalized interfacial bonding, k_{12}/k_{11} for a chain model with $m_1 = 2m_2$ and $k_{11} = k_{22}$ for a phonon with frequency $(= 0.532 \text{ (k/m)})(1/2)$.

A calculation based on this model shows that the interfacial phonon-transmission coefficient for a typical phonon representing those carrying the majority of the heat strongly increases with increasing interfacial stiffness,⁴ as shown in Fig. 1. Furthermore, the transmission coefficient saturates at strong bonding at the value of 0.970, which is the same as given by the prediction of the AMM. This result shows that the interfacial conductance is strongly affected by the interfacial bonding and only when the bonding is sufficiently strong does the interfacial conductance reach values predicted by AMM. Alternatively, one can tune interfacial conductance by controlling interfacial bonding strength instead of controlling bulk properties.

In the context of fully three-dimensional models, Prasher and coworkers⁸ developed an analytical extension of the AMM that includes the effects of weak interface bond-spring constants; in this model an increase of the conductance is observed with increasing bond stiffness and then saturation. Similar observations were made for three-dimensional lattice models by Young and Maris who studied the effect of interfacial bonding and the phonon DOS on the interfacial thermal conductance between two FCC lattices using lattice-dynamics calculation.⁶

Motivated by the fact that interfacial bonding plays an important role in interfacial transport, we use MD simulations and model epitaxial interfaces to systematically investigate the role of interfacial stiffness on the interfacial conductance. We define here interfacial stiffness S as normal to the interface elastic constant $S = \partial P_{zz} / \partial \varepsilon_{zz}$, where P_{zz} is the normal to interface stress and ε_{zz} is interfacial strain. MD simulations can be easily adjusted by changing the strength of bonds across the interface.^{6,9} However, we will also use pressure to tune interfacial stiffness—this is motivated by the fact that such an approach can be realized in experiment.

The remainder of this paper is organized as follows. In the next section the model and the simulation methods are described; in Sec. III simulation results are presented and discussed. A summary and conclusion are presented in the last section.

II. MODEL AND SIMULATION METHODOLOGY

Our simulation structure is composed of two crystalline-cubic fcc blocks, as shown in Fig. 2(a). All interatomic interactions are modeled with the 12-6 Lennard Jones (LJ) potential:

$$E = 4\varepsilon \left[\left(\frac{\sigma}{r} \right)^{12} - \left(\frac{\sigma}{r} \right)^6 \right], \quad (5)$$

where ε is the depth of the potential well and σ is the distance parameter. The LJ potential is used because it is simple, it stabilizes fcc structure, and its anharmonicity allows the stiffness of the interface to be tunable by pressure. LJ potential and a similar interfacial model were used to study the anharmonic effects in heat transfer from metal to nonmetal substrates by Stoner and Maris.⁹ In our studies the same LJ parameters, $\varepsilon_1 = \varepsilon_2 = 1.0$, $\sigma_1 = \sigma_2 = 1.0$ (in LJ units) are used for both blocks, and consequently each block has the same number density. Using ε for the interfacial interactions can be different from the corresponding bulk value. In some simulations we will use ε of the interface as an adjustable parameter to study the effect of the interfacial bonding strength on the interfacial transport. The ratio of atomic masses is 2:1 in all simulations.

Periodic boundary conditions are used in all three dimensions, leading to two epitaxial interfaces in the simulation cell. Each block of atoms is comprised of $5 \times 5 \times 5$ cubic unit cells,

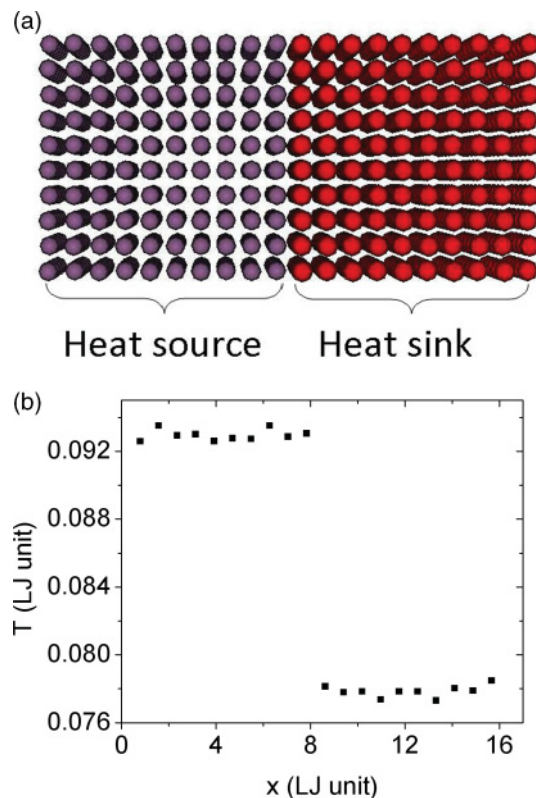


FIG. 2. (Color online) (a) Atomic structure of the simulation cell. A constant power heat source is applied to all atoms in one block of atoms and equal power heat sink is applied to all atoms in the other block of atoms. (b) Steady-state temperature profile (in reduced LJ unit $T^* = kBT/\varepsilon_{11}$). A temperature drop at the interfaces allows us to determine interfacial thermal conductance.

and each block contains 500 atoms. We performed several simulations on a system 40% larger in all three dimensions, and values of the interfacial conductance are within $\pm 5\%$ of those obtained in simulations of the primary system.

The direct method¹⁰ for computing thermal conductance by MD is used to study the thermal conductance at the interface. One of the blocks is set as heat source and another as heat sink, as illustrated in Fig. 2(a). Constant heat power is added to the heat source and removed from the heat sink by scaling velocities of the atoms in the heat source and heat sink regions at every time step. The temperature profiles of the two blocks are monitored to calculate the temperature drop at the interface difference and hence the thermal conductance [see Fig. 2(b)].

Before the heat flux is imposed, the system is equilibrated at constant pressure and has a temperature of 300 K for 100,000 MD steps (each step is 0.00333τ , where τ is LJ reduced-time unit). Then, the global thermostat is turned off, the volume of the simulation cell is fixed, and the local heat source and sink are applied. A steady state is established after $\sim 100,000$ MD steps, and the temperatures of the blocks are obtained by time averaging over $\sim 800,000$ MD steps.

Interfacial conductance G is calculated from the following equation:

$$G = \frac{P}{2A\Delta T}, \tag{6}$$

where P is the heating power, A the cross-sectional area of the interface, and ΔT is the temperature drop at the interfaces. The factor of 2 results from the presence of two interfaces due to use of periodic-boundary conditions. We report interfacial conductance in units of $\varepsilon\tau^{-1}\sigma^{-2}T^*$, where ε is reduced LJ energy, τ reduced LJ time, σ reduced LJ length, and T^* the reduced LJ temperature, as defined in the caption of Fig. 2(b).

III. RESULTS AND DISCUSSION

A. Effect of pressure on interface conductance

We first explore the effect of system pressure on interfacial conductance. We consider both weak and strong interfaces. For the weakly bonded interface we use $\varepsilon_{\text{interface}} = 1/30 \varepsilon_1$. Calculated thermal conductance as a function of pressure in this case is shown in Fig. 3 (open circles). As can be seen, conductance increases approximately linearly with the applied pressure and then gradually saturates. As we subsequently show, the increase of the interfacial conductance is due to an anharmonicity-related increase of the interfacial stiffness.

The interfacial stiffness is defined as the slope of the normal-to-interface pressure versus interfacial-strain curve, obtained as follows. In equilibrium simulations (without heat sources and sinks), we monitor interfacial strain versus pressure, as shown in Fig. 4(a). The strain is calculated from the change in the separation of the two atomic planes adjacent to the interface. In fact, as shown in Fig. 4(b), the interfacial stiffness increases more or less linearly with pressure, which demonstrates that the underlying reason for the increasing interfacial conductance is the increase of the interfacial stiffness.

The simulations described previously were performed with the interfacial bonding much weaker than the bulk bonding. To model a stronger interface we performed simulations where

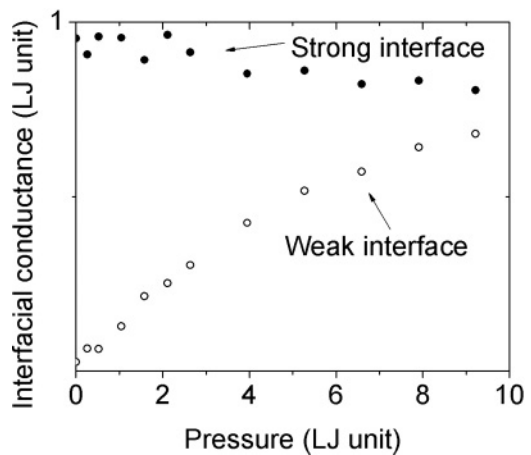


FIG. 3. Interfacial conductance versus pressure for weak interface (open circles) and strong interface (solid circles).

$\varepsilon_{\text{interface}} = \varepsilon_1$. The calculated conductance as a function of pressure for this is shown in Fig. 3 (solid circles). For this case interfacial conductance does not increase with pressure as for the weak interface (see Fig. 3, open circles) but is approximately constant and, in fact, decreases slightly with pressure.

This decrease is puzzling considering that for this system both interfacial modulus and modulus of materials 1 and 2

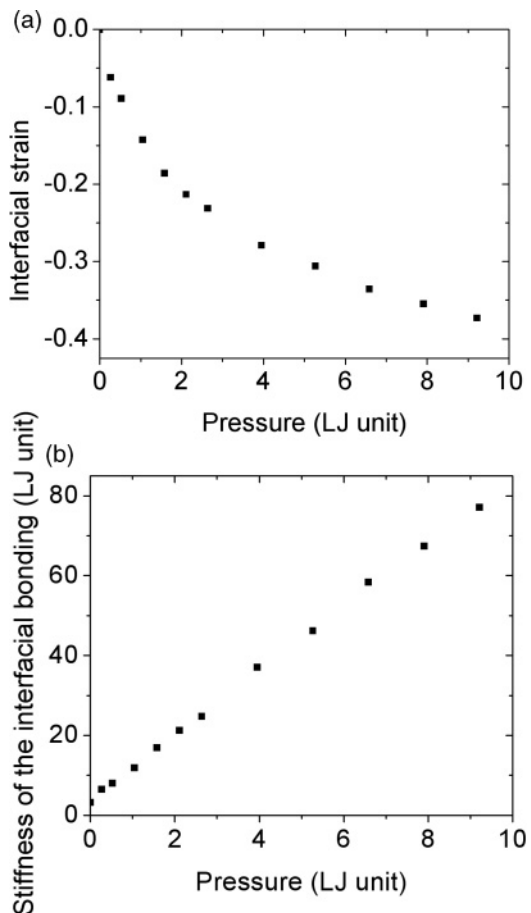


FIG. 4. (a) Pressure versus interfacial strain for the weak interface. (b) Interfacial stiffness as a function of pressure.

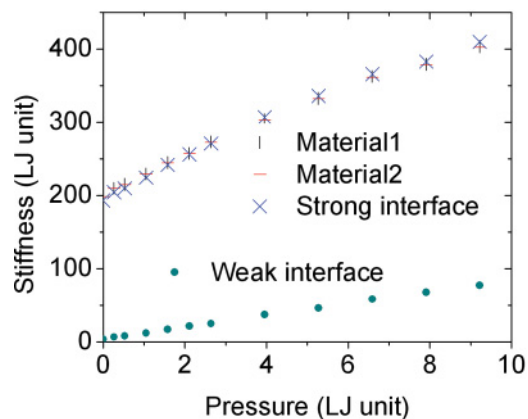


FIG. 5. (Color online) Stiffness versus pressure of material-1 (\circ), material-2 (\square), weak interface (\bullet), and strong interface (\times).

increase with pressure due to anharmonicity of the interatomic potential. In fact interfacial stiffness and bulk modulus are exactly the same for the strong interface at all pressures (see Fig. 5) as the atomic potential for the interfacial interactions is the same as the bulk interactions. Therefore, since all interactions become progressively stiffer at the same rate, both the phonon frequencies and their group velocities increase with increasing pressure. At first sight, this implies, according to Eq. (2), that pressure should increase interfacial conductance. One possible explanation is that phonon transmission coefficients are decreasing with increasing pressure; this possibility will be discussed in Sec. III C.

B. Effect of interface bonding on conductance

Since we demonstrated previously that the pressure change is effectively changing the stiffness of the interatomic bonds, we also performed MD simulations in which we maintained zero-hydrostatic pressure and varied stiffness of the interfacial bonding by changing ϵ for the interfacial interactions. This approach mimics change of interfacial interactions by change of interfacial chemistry. It also allows for independent exploration of the role of interfacial interactions versus bulk ones, while in the case of pressure-induced stiffness, both stiffness of the interface and the bulk stiffness change at the same time. Therefore, to separate bulk and interfacial effects and compare against results obtained in pressure simulations, we performed two sets of simulations in which we vary ϵ . In the first set, only the interfacial ϵ is changed; in the second set, both the bulk and interfacial ϵ are changed, as prescribed by the interfacial stiffness data shown in Fig. 5.

The simulation results are summarized and compared with pressure simulation data in Figs. 6(a) and 6(b). In the case of the weak interface [Fig. 6(a)], an increase of the bond stiffness, either via pressure or via bonding-energy parameter, always makes the interfacial conductance increase. The change in the data induced by pressure and the change in the data induced by changes in the stiffness produced directly by changes in both the interfacial and bulk-bonding parameters collapse onto each other up to pressures of 1.58 LJ units, indicating that the two methods for modifying the interface stiffness are equivalent. At larger stiffness both bulk and interfacial bonding-increased stiffness results in a lower conductance increase than the

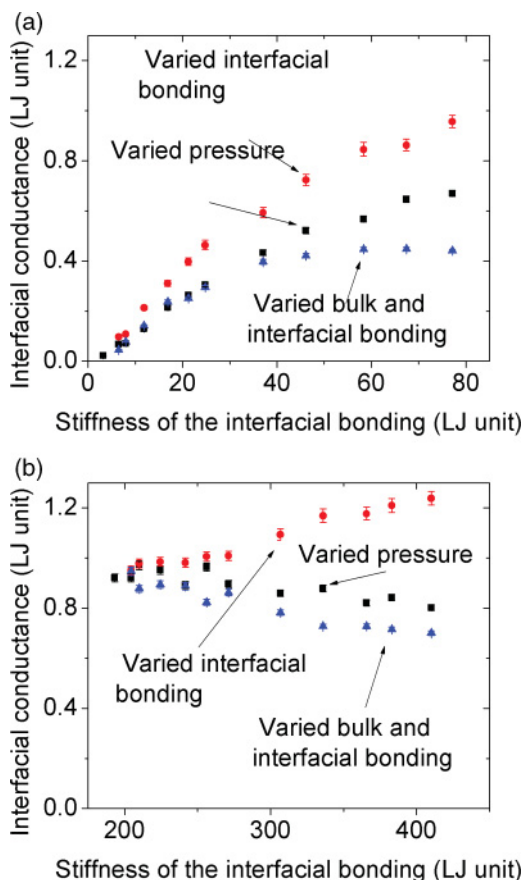


FIG. 6. (Color online) Interfacial conductance as a function of stiffness for (a) weak and (b) strong interfaces. Three data sets in each case correspond to pressure-induced change (solid squares), corresponding bulk modulus, and interfacial stiffness-induced change (solid triangles) and interfacial bonding-only induced change (solid circles).

pressure-increased stiffness. This might be associated with the fact that at higher pressures the interatomic distances across the interface become significantly shorter, thus enhancing energy transport. In the case when only interfacial bonding stiffness increases, the increase of the conductance is the largest. This implies that while the increasing interfacial bonding increases the conductance, an increase of the bulk modulus decreases the conductance.

For strong interfaces [Fig. 6(b)], the interfacial conductance increases when the interfacial ϵ alone is increased; it decreases when both the stiffness of the interfacial bonding and the bulk is increased either via pressure or directly via the bonding energy parameters. This is consistent with the fact that an increase of the bulk modulus tends to reduce interfacial conductance for our model system, and in the case of a strong interface, this effect dominates. By contrast, in the case of the weak interface, the rapidly increasing stiffness of the weak interface dominates the overall behavior, leading to increased interfacial conductance.

C. Phonon DOS overlap and interfacial conductance

Results presented in the previous section indicate that for the weak interface changes in bulk modulus with increasing

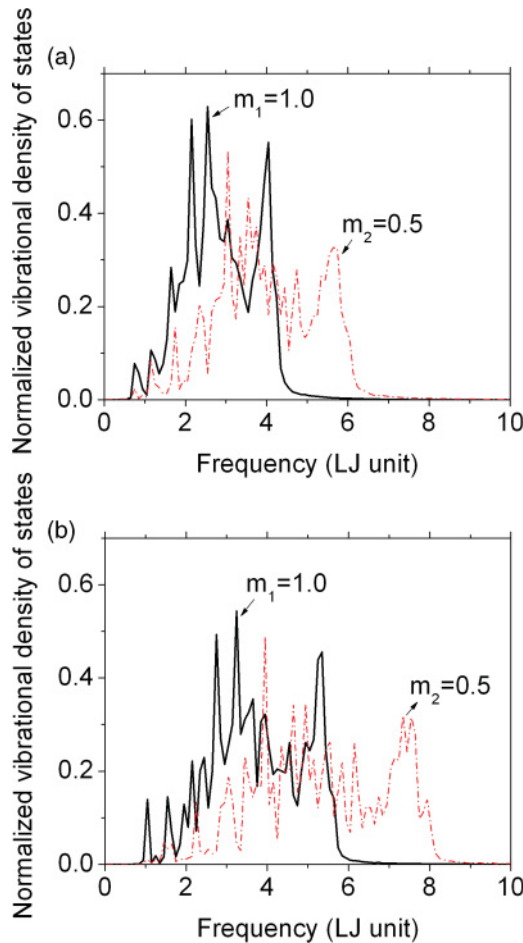


FIG. 7. (Color online) Normalized DOS for the two types of atoms at (a) zero pressure and (b) pressure of 9.22 (LJ units). DOS for the lighter atoms extends to higher frequency and there is less overlap at lower frequencies.

pressure [Fig. 6(a)] produce a smaller increase in interfacial conductance rather than only changing interfacial stiffness [Fig. 6(a)]; for the strong interface, changes in bulk properties even produce a slight decrease in interfacial conductance [Fig. 6(b)]. This behavior is most likely due to changes in phonon-transmission coefficients. For harmonic phonon-scattering processes, the overlap of phonon DOS of the materials on two sides of the interface dominate thermal transport across the interface. To analyze the relationship between DOS overlap and the interfacial conductance, we evaluated phonon DOS in each block as a function of pressure. Phonon DOS is calculated by Fourier transform of the atomic velocity autocorrelation function.¹¹ The resulting phonon DOS for atoms of both blocks are shown for both zero pressure [Fig. 7(a)] and the highest pressure studied [Fig. 7(b)]. Since the only difference between the two blocks is the atomic mass, the DOS for heavy atom regions is a scaled-down version of the light mass region with the highest frequency proportional to the inverse of the square root of mass.

In the harmonic approximation the interfacial conductance depends on the overlap of the DOS from each sides of the interface.¹² The overlap of the DOS is given by the integral

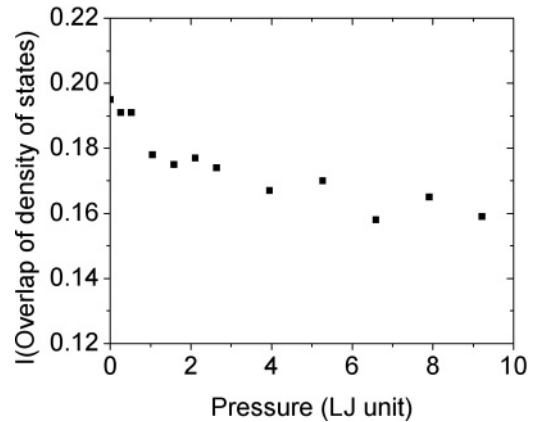


FIG. 8. Integral of the product of DOS versus pressure for the strong interface.

of the product of the DOS of the two bulk regions over the frequency with nonzero overlap value:

$$I = \int_0^{f_h} D_1(\omega)D_2(\omega)d\omega, \tag{7}$$

where $D_1(\omega)$ and $D_2(\omega)$ are phonon DOS for block 1 and 2, respectively, and f_h is the cutoff frequency of the DOS for the heavier atom region.

Figure 8 shows the value of the overlap integral as a function of pressure for the strong interface. The integral value decreases with pressure indicating a decrease in the overlap of DOS. Therefore, the number of harmonic-conductance channels between vibrations with the same frequency decreases with increasing pressure. This is a likely explanation of why, in this case, the interfacial conductance decreases with increasing pressure, despite the fact that with increasing pressure, the stiffness of both interfacial and bulk interactions increases.

To provide a further demonstration that the overlap in the DOS is an important factor for predicting the behavior of the

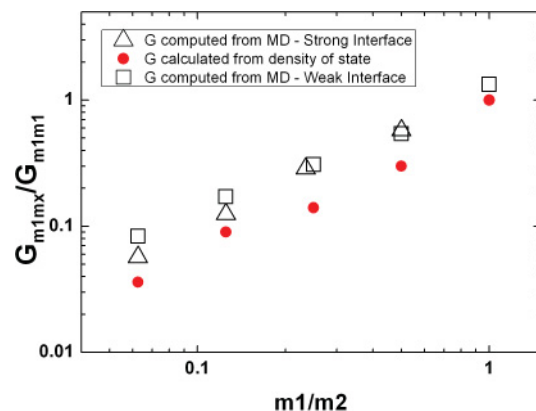


FIG. 9. (Color online) Normalized interfacial conductance of weak interfaces (open squares) and strong interfaces (open triangles) as a function of mass ratio (m_1/m_2) computed from MD and from overlap of DOS (solid circles). The weak interface data is normalized with G_{weak}, m_1, m_1 and the strong interface data with the same factor multiplied by the ratio of the interfacial bonding energy parameters, $\epsilon_{strong}/\epsilon_{weak}$.

interfacial thermal transport, we perform simulations where LJ force-field parameters for the bulk materials and the interface are kept constant (weak interface: $\epsilon_{12} = 1/30 \epsilon_1$, $\sigma_{12} = \sigma_1$; strong interface: $\epsilon_{12} = \epsilon_1$, $\sigma_{12} = \sigma_1$), while the atomic mass ratio for the two blocks is varied. Mass affects atomic-vibration frequencies, therefore overlap between the DOS depends on the mass ratio. Normalized interface conductance obtained from these simulations as a function of mass ratio is shown (weak interface: open squares; strong interface: open triangles) in Fig. 9. The conductance of weak interface is normalized to the value of the conductance of weak interface with mass ratio of unity; the strong interface data with the same factor is multiplied by the ratio of the interfacial bonding-energy parameters $\epsilon_{\text{strong}}/\epsilon_{\text{weak}}$. As the mass ratio increases toward unity, the two materials become more similar, and the thermal conductance of the interface increases.

In Fig. 9 we also show the overlap of the DOS normalized by the overlap for the case of the mass ratio of 1 (solid circles). The data for normalized DOS overlap clearly follow the data for the normalized interfacial conductance. These results demonstrate the quantitative relationship between the DOS overlap and the interfacial conductance.

IV. CONCLUSION

We investigated the effect of interfacial stiffness on the interfacial thermal conductance using nonequilibrium MD simulations applied to a simple LJ system. We modified bonding at the interface in two ways: application of pressure to the entire system and directly varying bonding across the interface by modification of the LJ force field.

Both weakly and strongly bonded interfaces were investigated as a function of applied pressure. In the case of weak interfaces the interfacial bonding dominates the change in interfacial conductance with pressure. The interfacial stiffness increases with increasing pressure; consequently, interfacial conductance initially increases proportionally to interfacial stiffness and then saturates. We believe that this result is very general and not limited to our model structure based on the following reasoning: (i) the soft bonds will become stiff with application of pressure; (ii) the interfacial conductance

with increasing bonding strength was reported in many publications.^{6,9} Furthermore, we conducted preliminary studies of two hetero-junctions, including a system of diamond-silicon and a system of aluminum-silicon carbide weakly bonded interfaces. Both systems exhibit similar behavior of conductance increasing with pressure at low and moderate pressures. At high pressures (~ 10 GPa) the situation can be more complicated as, e.g., silicon exhibits bulk structure-phase change. These results will be described in detail elsewhere.

For the strongly bonded interface, thermal conductance of the interface is almost pressure independent and in fact slightly decreases with increasing pressure. By evaluating the overlap of DOS of the two materials forming the interface, we demonstrated that this small decrease of conductance can be explained by decreasing overlap between vibrational DOS. Therefore, changes of bulk modulus with pressure in each half of the structure dominate the changes in interfacial conductance for the strong interface. The conclusion that the interfacial thermal conductance of the strongly bonded interfaces decreases with pressure is likely potential and/or model-structure sensitive, as the overlap of the vibrational spectra can in principle increase or decrease with increasing pressure. However, the fact that for strong interfaces the pressure dependence is weak is likely a general behavior.

We also directly varied the interfacial bonding as well as bulk and interfacial bonding at zero pressure and determined that pressure-induced changes are essentially equivalent to bonding-induced changes. Our results are consistent with numerical calculations based on Green's function formalism and the Caroli formula. Finally, we verified the importance of DOS overlap in controlling interfacial thermal conductance by computing the effect of variation of mass ratio on conductance, showing it is correlated with the extent of DOS, which is fully consistent with lattice-dynamics calculations by Stoner and Maris.⁹

ACKNOWLEDGMENT

This work was supported by the U.S. Air Force Office of Scientific Research Grant No. MURI FA9550-08-1-0407

*keblip@rpi.edu

¹S. Shenogin, L. P. Xue, R. Ozisik, P. Keblinski, and D. G. Cahill, *J. Appl. Phys.* **95**, 8136 (2004).

²E. T. Swartz and R. O. Pohl, *Rev. Mod. Phys.* **61**, 605 (1989).

³S. Petterson and G. D. Mahan, *Phys. Rev. B* **42**, 7386 (1990).

⁴M. Hu, P. Keblinski, and P. K. Schelling, *Phys. Rev. B* **79**, 104305 (2009).

⁵S. T. Huxtable, D. G. Cahill, S. Shenogin, L. Xue, R. Ozisik, P. Barone, M. Usrey, M. S. Strano, G. Siddons, M. Shim, and P. Keblinski, *Nat. Mater.* **2**, 731 (2003).

⁶D. A. Young and H. J. Maris, *Phys. Rev. B* **40**, 3685 (1989).

⁷C. Caroli, R. Combescot, P. Nozieres, and D. Saint-James, *J. Phys. C* **4**, 916 (1971).

⁸R. Prasher, *Appl. Phys. Lett.* **94**, 041905 (2009).

⁹R. J. Stoner and H. J. Maris, *Phys. Rev. B* **48**, 16373 (1993).

¹⁰P. K. Schelling, S. R. Phillpot, and P. Keblinski, *Phys. Rev. B* **65**, 144306 (2002).

¹¹M. P. Allen and D. J. Tildesley, *Computer Simulation of Liquids* (Oxford Science Publications, New York, 1986).

¹²C. T. Chang, J. P. Sethna, A. N. Pasupathy, J. Park, D. C. Ralph, and P. L. McEuen, *Phys. Rev. B* **76**, 045435 (2007).